Dalton Transactions

Accepted Manuscript

ROYAL SOCIETY OF CHEMISTRY

www.rsc.org/dalton

ARTICLE TYPE www.rsc.org/xxxxxx | XXXXXXXX

An organic-inorganic hybrid semiconductor material based on lindqvist polyoxomolybdate and tetra-nuclear copper complex containing two different ligands

Zhi-Kun Qu,[a] Kai Yu,*[a,b] Zhi-Feng Zhao,[a,b] Zhan-hua Su,[a,b] Jing-Quan Sha,[c] Chun-Mei Wang,[a,b] Bai-Bin Zhou,*[a,b]

Received (in XXX, XXX) Xth XXXXXXXXX 200X, Accepted Xth XXXXXXXXX 200X
First published on the web Xth XXXXXXXXX 200X
DOI: 10.1039/b000000x

A 3D organic–inorganic hybrid compounds based on the Lindqvist-type polyoxometalate, $[\{Cu(phen)\}_3\{Cu(\mu_2\text{-}ox)_3\}\{Mo_6O_{19}\}]$ (**1**) (phen = 1,10-phenanthroline, ox = oxalate), has been synthesized under hydrothermal conditions and structurally characterized by elemental analysis, IR, TG, PXRD, XPS, UV-vis, and single-crystal X-ray diffraction. In compound **1**, three $C_2O_4^{2-}$ ligands bridge one Cu atoms and three Cu(phen) fragments to form a tetra-nuclear copper(II) coordination complex $[\{Cu(phen)\}_3\{Cu(\mu_2\text{-}ox)_3\}]^{2+}$ unit. The six-node $[Mo_6O_{19}]^{2-}$ clusters are interweaved by the 6-connected tetranuclear copper(II) complexes unit into a intricate 3D network structure, exhibiting a $4^{12}\bullet6^3$-nbo (sodium chloride-type) topology. Compound **1** represents the highest connectivity of Lindqvist-type POM hybrid materials. The electrochemical behavior of **1**-CPE has been investigated in detail. Furthermore, diffuse reflectivity spectrum of **1** reveals presence of an optical band gap and the nature of semiconductivity with a large energy gap. Magnetic susceptibility study reveals predominant antiferromagnetic interactions between the Cu^{II} bridge units.

Introduction

The rational design and synthesis of organic-inorganic hybrid materials based on the polyoxometalate (POM) building blocks is still an appealing subject due to their rich structural chemistry and widespread potential applications in catalysis,[1] molecular adsorption,[2] electromagnetic functional materials,[3] biological chemistry,[4] and photochemistry.[5] A current research interest in this field is the introduction of secondary organic and/or transition metal complex moieties, which can serve as bridging ligands, and graft into the framework of POM via covalent bonds. In this way, organic components can dramatically influence microstructure of hybrid materials. In addition, the synergic interactions between organic and inorganic components may be exploited in the preparation, which make hybrid materials exhibit composite properties. Thus, construction of such hybrid materials involves the selection and design of organic and inorganic building units as well as the control of synergic interactions between the counterparts.

As a unique class of metaloxide clusters, the Lindqvist hexamolybdate cluster $[Mo_6O_{19}]^{2-}$ represents one of the ideal building blocks to construct the Organic-inorganic hybrids assemblies. Recently, two effective methods have been exploited for the hybrid of the Lindqvist POMs. One approach is to replace the surface oxygen atoms of $[Mo_6O_{19}]^{2-}$ with various nitrogenous ligands. With the methods, the six terminal oxygen and some bridging oxygen atoms in the hexamolybdate cluster can be partially or completely substituted by nitrogenous species. Wei et al have opened an effective way to functionalize Lindqvist POMs with organoimido ligands.[6] The other one is to build connections between the surface oxygen atoms of $[Mo_6O_{19}]^{2-}$ and various organic units through secondary metal sites of coordination complex subunits. In contrast, hybrid materials derived from the latter method are still less common and only a minority of the kinds of hybrids have been reported. Hitherto only one monosubstituted,[7] two disubstituted,[8] one tetrasubstituted,[9] and one hexadsubstituted derivatives[10] of such kinds of hybrids have been synthesized and structurally characterized. Therefore, multisubstituted covalent organic–inorganic hybrids have been rarely reported. The synthesis and exploration of 3D high-connected hybrids based on Lindqvist-type POM still remains a great challenge.

On the other hand, the organic moieties play an important role in adjusting the structures of the inorganic–organic compounds. In recent years, the assembly system containing two or more organic bridging ligands has been widely adopted to generate new complexes with diversified topologies and interesting properties. As is known, Oxalate ligands bear more flexible coordination fashion and excellent coordination ability, which is favor to converge and bridge the transition metal ions forming multi-nuclear coordination polymers. Moreover, the introduction of a second aromatic organonitrogen ligand, such as 1,10-phen, often causes the system to produce many interesting structures. As a didentate ligands, 1,10-phenanthroline rings not only can make frameworks robust but also have the potential to form π-electron system. Furthermore, the transition metal copper(II) ions have been widely used as the linking units to construct the hybrid compounds due to their relatively strong coordination abilities with both terminal O atoms of POM and N atoms of organic ligand, as well as for their capacity to adopt various coordination number. In fact, Cu(II) ions containing paramagnetic spin-couple bear interesting magnetic properties, which are easy to form unique magnetic clusters under the inducement of oxalate ligands.

Thus, it is possible to conduct unusual magnetic interaction between POMs building block and copper metal complex.

Based on aforementioned considerations, tetra-nuclear copper complex as linkers is introduced into $\{Mo_6O_{19}\}$ system under hydrothermal conditions via employing mixed ligand ox and phen to assemble Bird's Nest-liked 3-D organic-inorganic hybrid, namely, $[\{Cu(phen)\}_3\{Cu(\mu_2\text{-}ox)_3\}\ \{Mo_6O_{19}\}]$ (**1**). Our result further suggests that oxalate is an excellent template reagent and linking unit to induce new 3D multi-nuclear POM-based hybrid assemblies.

Experimental

Materials and physical measurements

All reagents were purchased commercially and used without further purification. Elemental analyses (C, H, and N) were performed on a Perkin-Elmer 2400 CHN Elemental Analyzer. Mo and Cu analyses were performed on a PLASMA-SPEC (I) inductively coupled plasma atomic emission spectrometer. The IR spectra were obtained on an Alpha Centaurt FT/IR spectrometer with KBr pellet in the 400-4000 cm^{-1} region. The thermal gravimetric analyses (TGA) were carried out in N_2 on a Perkin-Elmer DTA 1700 differential thermal analyzer with a rate of 10 °C/min. XRD patterns were collected on a Rigaku Dmax 2000 X-ray diffractometer with graphite monochromatized Cu K_α radiation (λ= 0.154 nm) and 2θ ranging from 5 to 50°. X-ray photoelectron spectroscopy (XPS) analyses were performed on a VG ESCALAB MK II spectrometer with an MgK_α (1253.6 eV) achromatic X-ray source. The vacuum inside the analysis chamber was maintained at 6.2×10^{-6} Pa during analysis. The UV-vis-NIR absorption spectroscopy was measured with a Cary 500 spectrophotometer. Diffuse reflectivity spectrum was collected on a finely ground sample with a Cary 500 spectrophotometer equipped with a 110 mm diameter integrating sphere. Diffuse reflectivity was measured from 200 to 1500 nm using barium sulfate ($BaSO_4$) as a standard with 100% reflectance. Electrochemical measurements were performed with a CHI660 electrochemical workstation. A conventional three-electrode system was used. The working electrode was a carbon paste electrode (CPE), a Pt wire as the counter electrode and Ag/AgCl (3M KCl) electrode was used as a reference electrode. Magnetic susceptibility data were collected over the temperature range of 2-300 K in a magnetic field of 1000 Oe on a Quantum Design MPMS-5 SQUID magnetometer.

Synthesis

$[\{Cu(phen)\}_3\{Cu(\mu_2\text{-}ox)_3\}\{Mo_6O_{19}\}]$ (1) A mixture of $(NH_4)_6Mo_7O_{24}\bullet 4H_2O$ (1.236 g, 1 mmol), $CuCl_2\bullet 6H_2O$ (0.243 g, 1 mmol), 1,10-phenanthroline(0.180 g, 1 mmol), oxalic acid (0.180 g, 2mmol) and water (18ml, 1mol) was stirred for 30 min. Then, the resulting suspension was sealed in a 30-mL Teflon reactor and heated at 160 °C for 3 days. After cooling to room temperature, Dark blue block crystals of **1** were isolated. The crystalline products were collected by filtration, washed with distilled water, and air-dried to give a yield of 45% (based on Mo). Elemental anal. Calcd (%) for $C_{84}H_{48}Cu_8Mo_{12}N_{12}O_{62}$ (M_r = 3876.94) (%): C, 26.02; H, 1.25; N, 4.04; Cu, 13.11; Mo, 29.70; Found (%): C, 26.08; H, 1.21; N, 4.08; Cu, 13.07; Mo, 29.74. Selected IR (KBr pellet, cm^{-1}): 3083 (br), 1628 (sh), 1510 (m), 1418 (w), 1310 (s), 938 (s), 813 (s), 701 (s).

X-ray crystallography

The crystal structure of compound **1** was determined from single-crystal X-ray diffraction data. Intensity data were collected on a Bruker SMART CCD diffractometer equipped with a graphite monochromatized Mo-K_α radiation (λ= 0.71073Å). The structure was solved by direct methods and difference Fourier map with SHELXL-97 program,[11] and refined by full-matrix least-squares techniques on F^2. Anisotropic thermal parameters were used to refine all non-hydrogen atoms. The positions of hydrogen atoms of organic molecules were calculated theoretically, and refined using a riding model. Hydrogen atoms of water molecules were not treated. The crystal data and refinement parameters of compounds **1** are summarized in Table **1**. The selected bond lengths and bond angles of compounds 1 are listed in Table S1.

Table 1. Crystal Data and Structure Refinement for **1**

Compound	**1**
Chemical formula	$C_{84}H_{48}Cu8Mo_{12}N_{12}O_{62}$
Formula weight	3876.94
T/K	293(2)
λ/Å	0.71073
Crystal system	Trigonal
Space group	*R-3c*
a/Å	14.9724(3)
b/Å	14.9724(3)
c/Å	80.713(3)
α/°	90.00
β/°	90.00
γ/°	120.00
V/Å^3	15669.5(8)
Z	6
D_{calc}/Mg m^{-3}	2.465
μ/mm^{-1}	3.090
F(000)	11208
crystal size/mm	0.18 x 0.18 x 0.16 mm
θ range/°	1.65–28.27
Reflections collected/ unique	31117 / 4326 [R(int) = 0.0452]
Data/restraints/parameters	4326 / 0 / 270
GOF on F^2	1.007
Final *R* indices [$I > 2\sigma(I)$][a]	R_1 = 0.0287, wR_2 = 0.0689
R indices (all data)[b]	R_1 = 0.0416, wR_2 = 0.0753

[a] $R_1 = \Sigma ||F_0|-|F_C|| / \Sigma |F_0|$; [b] $wR_2 = \Sigma [w(F_0^2-F_C^2)^2] / \Sigma [w(F_0^2)^2]^{1/2}$

Results and Discussion

Crystal Structure

X-ray Single-crystal structural analyses reveal that compound **1** crystallizes in the trigonal system, space group R-3c. Compound **1** consists of $[Mo_6O_{19}]^{2-}$ anions and the tetra-nuclear copper fragment $\{[Cu(phen)]_3[Cu(\mu_2\text{-}ox)_3]\}^{2+}$ (Fig. 1). The Linquist structure $[Mo_6O_{19}]^{2-}$ consists of a central oxygen atom which is surrounded by six Mo atoms in an octahedral geometry. Each metal Mo has one terminal oxygen atom, and shares additional four μ_2-oxygen atoms with adjacent metal atoms.

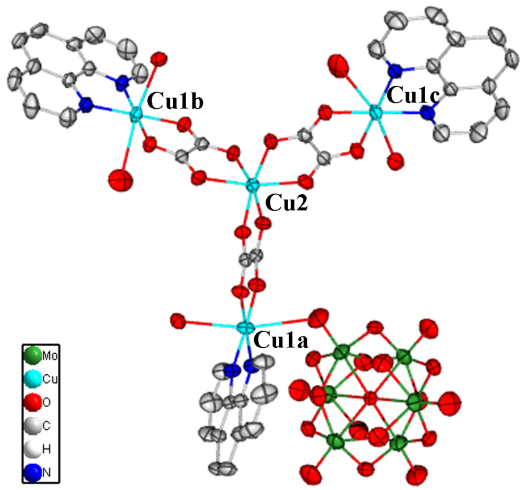

Figure 1 ORTEP view of the basic units in compound 1 with 50% thermal ellipsoids.

As shown in Fig.2(a), the tetra-nuclear copper fragment of **1** contains two kinds of crystallology independent copper atoms (Cu1 and Cu2), which exhibit the hexa-coordination environment. The Cu2 locating the centre of octahedral geometry is defined by six O atoms derived from three ox ligands, with the bond lengths of Cu2-O 2.080(2) Å. Cu1 exhibits distortional octahedral geometry which is defined by two N atoms from a phen, two O atoms from an ox ligand, and two terminal O atoms from two adjacent $Mo_6O_{19}^{2-}$ anions with the distance of Cu2-Ot: 2.495(2) and 2.667(3) Å, Cu2-Oox: 1.952(2) and 1.957(2) Å, Cu2-N: 1.967(3) and 1.981(3). In such connection mode, three $C_2O_4^{2-}$ ligands bridge one Cu atoms and three Cu(phen) fragments to form a tetra-nuclear copper(II) coordination complex unit. Each $[Mo_6O_{19}]^{2-}$ cluster serves as hexa-dentate ligand coordinating to six Cu1 centers through all the terminal oxygen atoms and further supports six tetra-nuclear complex $\{[Cu(phen)]_3[Cu(\mu_2\text{-}ox)_3]\}^{2+}$ unit via Cu1 atoms (Fig.2(b)).

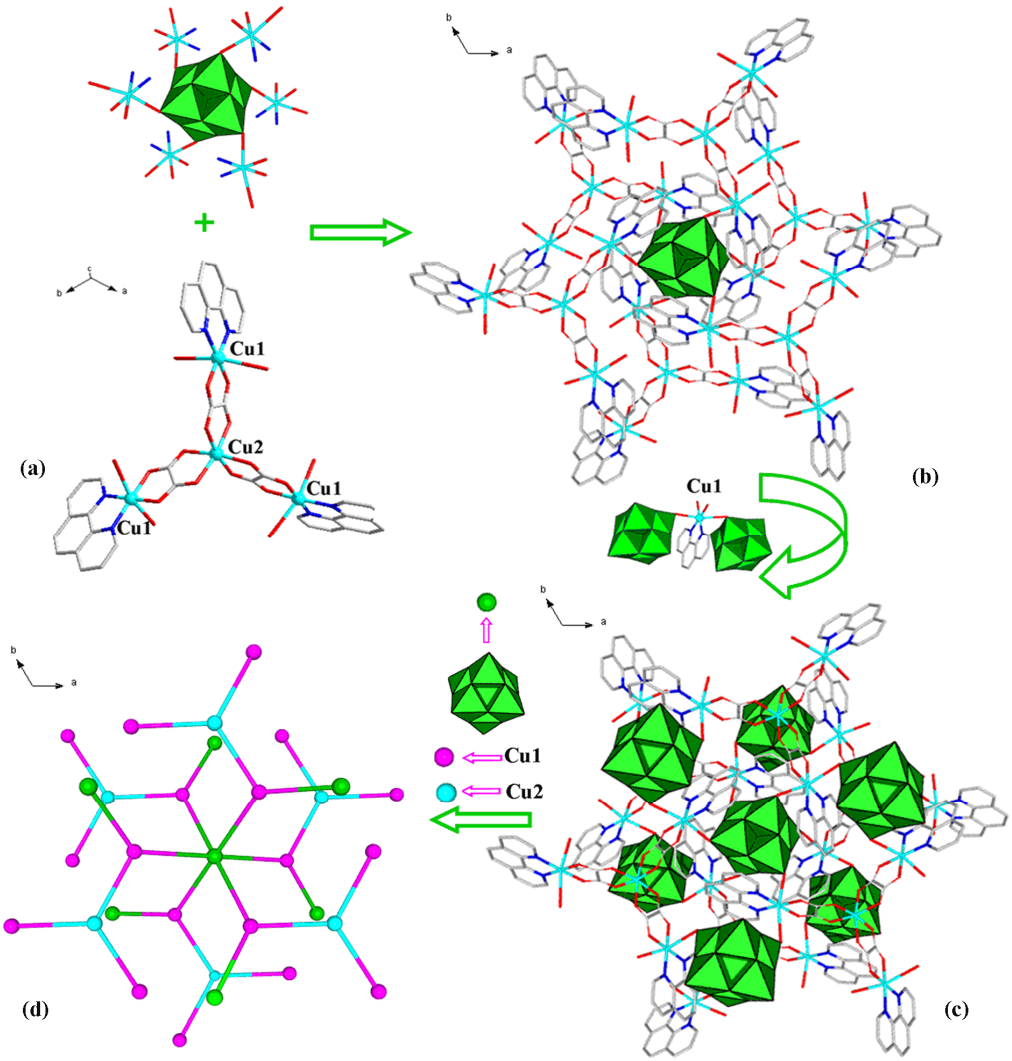

Figure 2. (a) Coordination environment of $Mo_6O_{19}^{2-}$ and $\{[Cu(phen)]_3[Cu(\mu_2\text{-}ox)_3]\}^{2+}$ in compound 1; (b) Each $[Mo_6O_{19}]^{2-}$ cluster supports six $\{[Cu(phen)]_3[Cu(\mu_2\text{-}ox)_3]\}^{2+}$ via the six Cu1-O bonds (peripheral $\{Mo_6O_{19}\}$ clusters are omitted for clarity); (c) Each $[Mo_6O_{19}]^{2-}$ cluster connects with six peripheral Linquist-type cluster and six tetra-nuclear copper(II) complex unit via Cu1 atoms; (d) View of the topology of Coordination environment of each $[Mo_6O_{19}]^{2-}$.Schematic illustration of the synthesis routes of complexes.

Moreover, each Cu1 links to two $[Mo_6O_{19}]^{2-}$ clusters, which result in each tetra-nuclear cooper complex joins to six Linquist clusters (Fig. S1). At the same time, Each $[Mo_6O_{19}]^{2-}$ cluster connects with six peripheral Linquist-type cluster via Cu1 atoms (Fig. 2(c) and Fig. 2(d)). The six peripheral $[Mo_6O_{19}]^{2-}$ clusters make up two parallel equilateral triangles which are located at the two sides of the central $[Mo_6O_{19}]^{2-}$ cluster (Fig. 3). In addition, an important feature of the structure is that three Cu1 atoms, one Cu2 atoms, two $C_2O_4^{2-}$ ligands and two $[Mo_6O_{19}]^{2-}$ polyoxoanions construct a polyhedron cavity with the dimension of 6.580×13.59 (Fig. 4). The apertures of the open network are filled by barrier-liked phen (shown in Fig.S2).

Figure 3. The six peripheral $[Mo_6O_{19}]^{2-}$ clusters make up two parallel equilateral triangles which are located at the two sides of the central $[Mo_6O_{19}]^{2-}$ cluster of the relationship between crystalline products of basket-type and different template reagent.

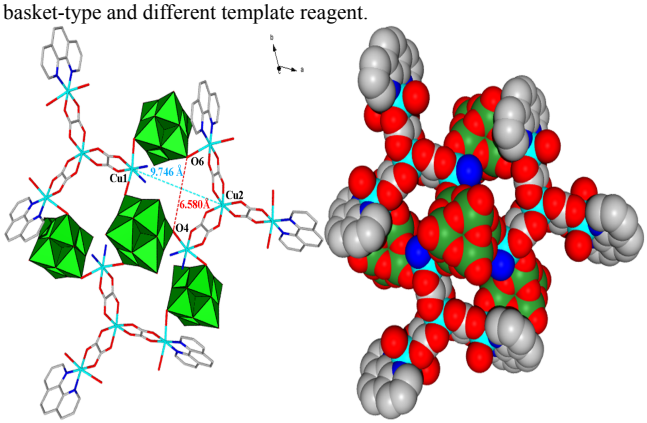

Figure 4. The polyhedron cavity constructed by three Cu1 atoms, one Cu2 atoms, two $C_2O_4^{2-}$ ligands and two $[Mo_6O_{19}]^{2-}$ polyoxoanions.

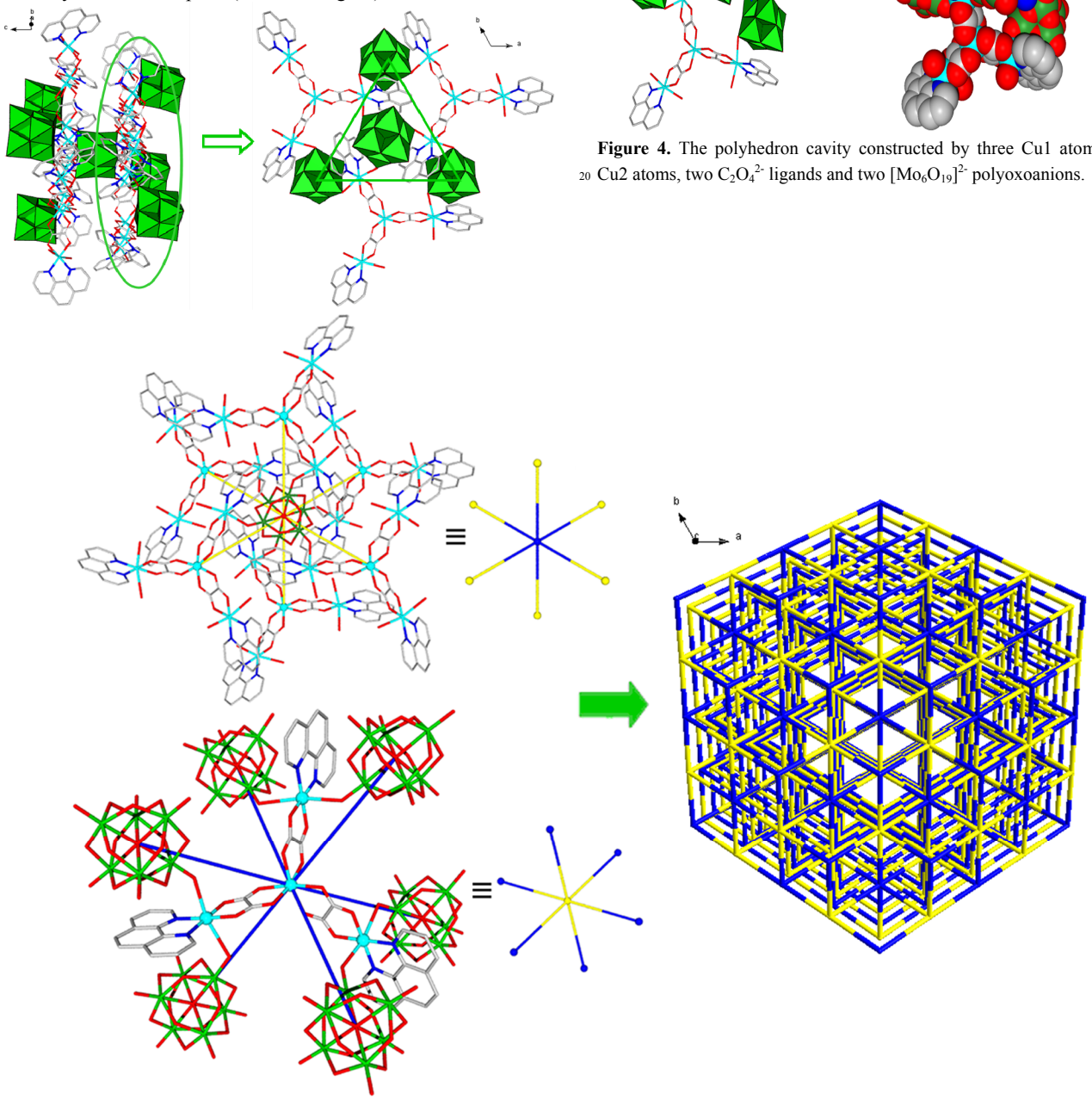

Figure 5. The 3D Bird's Nest-liked structure and $4^{12}•6^3$-nbo (sodium chloride-type) topology of compound **1**.

Most intriguing structural character is that the hexad-node $[Mo_6O_{19}]^{2-}$ clusters are interweaved by the 6-connected tetranuclear complexes unit into an intricate 3D network structure exhibiting a $4^{12}.6^3$-nbo (sodium chloride-like) topology (Fig. 5). In this simplification, the blue 6-connected nodes are $[Mo_6O_{19}]^{2-}$ cluster (O1 and O9 as central atom), the yellow 6-connected ones are tetranuclear complexes $\{[Cu(phen)]_3[Cu(\mu_2\text{-}ox)_3]\}^{2+}$ unit (Cu2 as central atom). The distances of Cu2-O1 are 9.416, 9.418, and 9.419 Å; the lengths of Cu2-O9 are 9.145, 9.147, and 9.148 Å. Compound **1** represents not only the highest connection Lindqvist-type hybrid but also the first 3D Lindqvist-type hybrid modified by tetra-nuclear copper(II) coordination complex. It is worth noting that $C_2O_4^{2-}$ ligands play dual role as both pillar and crucial linkers of tetra-nuclear units, while phen ligands are located in the cavities of 3D hybrid materials to stabilize tetra-nuclear copper cluster and overall 3D open framework. Thus, the ligands are important template reagent to induce the formation of the tetra-nuclear copper segments and interlaced 3D network structure. According to bond valence calculation,[12] all molybdenum atoms show +VI oxidation states and copper atoms are in +II oxidation states, which is also proved by charge neutrality.

Spectroscopic and Thermal Analyses:

In the IR spectrum of **1** (Fig. S3), the characteristic peaks at 802 and 941cm^{-1} are attributed to the ν(Mo-O-Mo) and ν(Mo=O) of the $Mo_6O_{19}^{2-}$ polyanions, respectively. Bands in the 1640-1110cm^{-1} region can be assigned to characteristic peaks of the ligands 1, 10-phen.[13] The bands between 1430-1310 and 802-717cm^{-1} are attributed to $\nu_{C\text{-}O}$ and $\nu_{C\text{-}C}$ oxalate symmetric stretching vibrations, respectively.[14a] The data imply that the oxalate anion serve as symmetric bi-chelated oxygen donor ligand, which is in agreement with the result of the X-ray analysis. The bands in the range of 482-442cm^{-1} can be assigned to ν_{as}(Cu-O) and ν_{as}(Cu-N) vibration.[14b]

The PXRD patterns for compound **1** are presented in Fig. S4. The diffraction peaks of both simulated and experimental patterns match in the key positions, indicating the phase purity of the compound. The differences in intensity may be due to the preferred orientation of the powder samples.

The oxidation states of Mo and Cu are further confirmed by X-ray photoelectron spectroscopy (XPS) measurements, which were carried out in the energy region of $Mo3d_{5/2}$, $Mo3d_{3/2}$, $Cu2p_{1/2}$, and $Cu2p_{3/2}$, respectively. The XPS spectrum of **1** presents two peaks at 932.7 eV and 953.2eV in the Cu2p region which should be ascribed to Cu^{2+} (Fig. S5a). The XPS spectra give two sharp peaks at 232.5 and 235.6 eV in the Mo3d region, which attributed to Mo^{6+} ions[15] (see Fig. S5b). All these results further confirm the valence sum calculations of compound **1**.

Thermogravimetric analysis (TGA) was performed at a rate of 10 ^{o}C•min^{-1} in the range of 35–500 ^{o}C on **1**(Fig. S6). In the TG curve of **1**, there exist two weight loss stages. In the temperature range of 150–200°C, the initial weight loss of 13.94% corresponds to the release of CO_2 from reduction of oxalic acid ligand under oxidation action of Cu(II), which in accordance with the calculated value of 13.25%. The second weight loss of 29.64% occurring between 225 °C and 290 °C is attributed to the release of the phen ligands (calcd. 29.81%). The whole weight loss (43.58%) is in good agreement with the calculated value (calcd. 43.06%). All these results are in agreement with aforementioned crystal structures.

The UV-vis-NIR absorption spectrum of compound 1 is shown in Fig. S7, and two characteristic absorption peaks at 227 and 326 nm can be detected. In the ultraviolet range, the lowest energy electronic transition at 326 nm was assigned to a charge-transfer transition from the terminal oxygen nonbonding HOMO to the molybdenum LUMO, which is in agreement with the Characteristic absorption peak of $[Mo_6O_{19}]^{2-}$ in the literature.[16]

Optical Band Gap

In order to explore the conductivity of compound **1**, the measurement of diffuse reflectivity for the powder sample was used to achieve its band gap (E_g). The band gap (E_g) was determined as the intersection point between the energy axis and the line extrapolated from the linear portion of the absorption edge in a plot of the Kubelka-Munk function F against energy E. As shown in Fig. 6, for this compound, the corresponding well-defined optical absorption associated with band gap (E_g) can be assessed at 3.12 eV. The reflectance spectrum measurements reveal the presence of an optical band gap and the nature of semiconductivity with a wide band gap for compound **1**. The band gap of 1 is larger than that of $(n\text{-}Bu_4N)_2\{trans\text{-}[Mo_6O_{17}(NAr)_2]\}$($E_g$ = 2.55 eV)[16] and closed to that of $[Ni_2(BIMB)_2(Mo^{VI}_4Mo^{V}_2O_{19})]$ (E_g =3.06 eV)[9] in previous literature. The extended tetra-nuclear complexes modified $\{Mo_6O_{19}\}$ hybrid structures are mainly responsible for its optical band gap.

Cyclic voltammetry

The cyclic voltammetric behavior for **1**-CPE in 1 M H_2SO_4 aqueous solution at different scan rates was recorded in Fig. 7. As shown in Figure S8, it can be clearly seen that three reduction peaks and two oxidation peaks appear in the potential range of +0.4 to -1.0 V at a scan rate of 20 mV·s^{-1}. One couple of redox peaks (II-II′) located at E_{pa} = 0.64 V and E_{pc} = 0.42 V are observed. These peaks correspond to one-electron oxidation and reduction steps involving Mo atoms, which are similar to analogous compounds reported in the literature.[9] The voltammetric response of $[Mo_6O_{19}][N(C_4H_9)_2]_2$ electrode (denoted to **2**-CPE) displays one couple of redox peaks at E_{pa} = 0.55 V and E_{pc} = 0.39V, which similar to that of II-II′ in **1**-CPE. This further indicates that redox reaction of II-II′ in **1**-CPE originates from Mo_6O_{19} (Figure S9). The last two reduction waves and their oxidation counterpart, a single oxidation process located at +0.12 V, are attributed to the redox processes of the Cu2+ centers[17]. The two reduction waves located at -0.09 and -0.06 V feature the reduction of Cu^{2+} to Cu^0, possibly through Cu^{1+} [17a]. Moreover, the cathodic peak potentials shift toward the negative direction and the corresponding anodic peak potentials shift to the positive direction with increasing scan rates. Additionally, the peak-to-peak separations between the corresponding anodic and cathodic peaks increased, but the average peak potentials do not change on the whole.

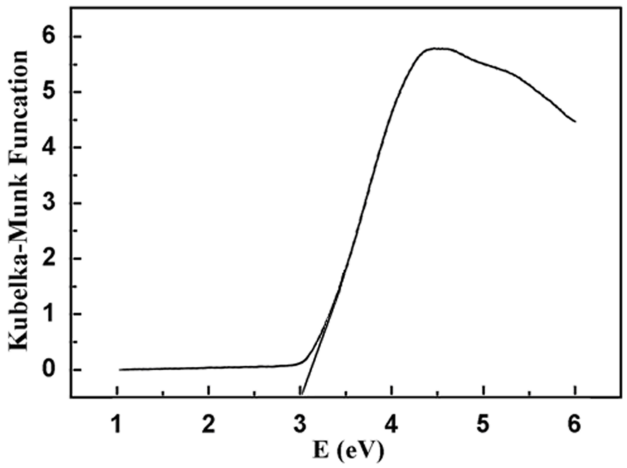

Figure6. K-M function versus energy (eV) curve of compound **1**.

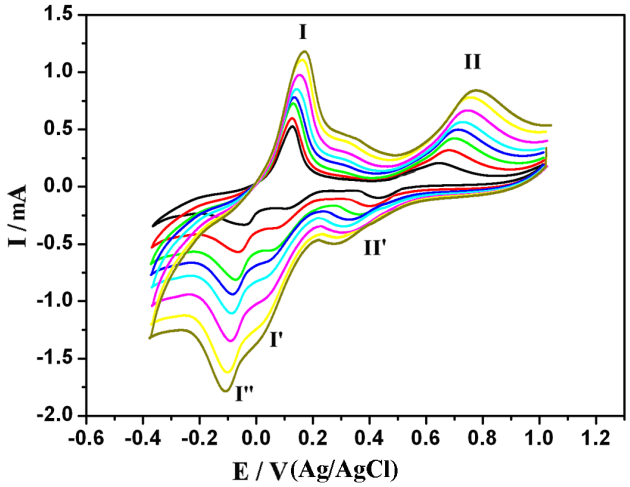

Figure7. The cyclic voltammograms of the **1**-CPE in 1 M H_2SO_4 at different scan rates (20, 50, 80, 110, 140, 170, 210, 240 mV•s^{-1}).

The variable temperature magnetic susceptibility of **1** were measured from 300 to 2 K at 1000 Oe and plotted as $\chi_M T$ and χ_M versus T, as shown in Figure 8. The χ_M increases continuously with decreasing temperature, and the curves of χ_M and $\chi_M T$ obey the Curie-Weiss law. The room temperature $\chi_M T$ value is 4.831cm^3•K•mol^{-1}, which is higher than the excepted for four noncorrelated Cu^{II} ions (1.67cm^3•K•mol^{-1}, considering g =2.10). It can be viewed that it is the result of combined action of the spin coupling and orbital contribution of Cu^{II} ions. When the systems is cooled, the $\chi_M T$ product decreases to a value of 2.027 cm^3•K•mol^{-1} at 15K. These behaviors indicate the presence of the antiferromagnetic coupling for **1**. At relatively low temperature (15K to 2K), the $\chi_M T$ product increases with decreasing temperature (as inner of Fig.8a), which might be mainly attributed to the presence of zero-field splitting. The behavior suggests that there exist overall antiferromagnetic interactions with the presence of zero-field splitting for Cu^{2+} ions in the compound **1**.

The magnetic mode of the tetra-nuclear copper(II) coordination fragment shown in Fig. 8(b) is an equilateral triangle, which is formed by the three equal isosceles triangles, and the isosceles parts are bridged by two oxalate ligands, respectively. The interactions of S_1-S_2 and S_1-S_3 are both described by the coupling constant J. The interaction of S_2-S_3 is given by the coupling constant J_1. In the presence of an external magnetic field, the spin Hamiltonian with $S_1=S_2=S_3=1/2$ for the tri-nuclear-copper fragment is given by $H=-2J(\hat{S}_1\bullet\hat{S}_2+\hat{S}_1\bullet\hat{S}_3)-2J_1\hat{S}_2\bullet\hat{S}_3$. The expression of χM for 1 is $\chi_M = (Ng^2\beta^2/4kT)\{1+\exp[(2J_1-2J)/kT]+10\exp[(2J_1+J)/kT]\}/\{1+\exp[(2J_1-2J)/kT]+2\exp[(2J_1+J)/kT]\}$, where N, β, and k have their usual meaning, g is a factor. The best-fitting parameters obtained from a simulation of the curve of χ_M versus T are J = -32.2 cm^{-1}, J_1= 65.0 cm^{-1} and g = 2.10 with the agreement factors, $R_\chi = [\sum\{(\chi_M)^{calcd}-(\chi_M)^{obsd}\}^2/\sum\{(\chi_M)^{obsd}\}^2] = 6.60\times10^{-4}$.

Magnetic Measurements

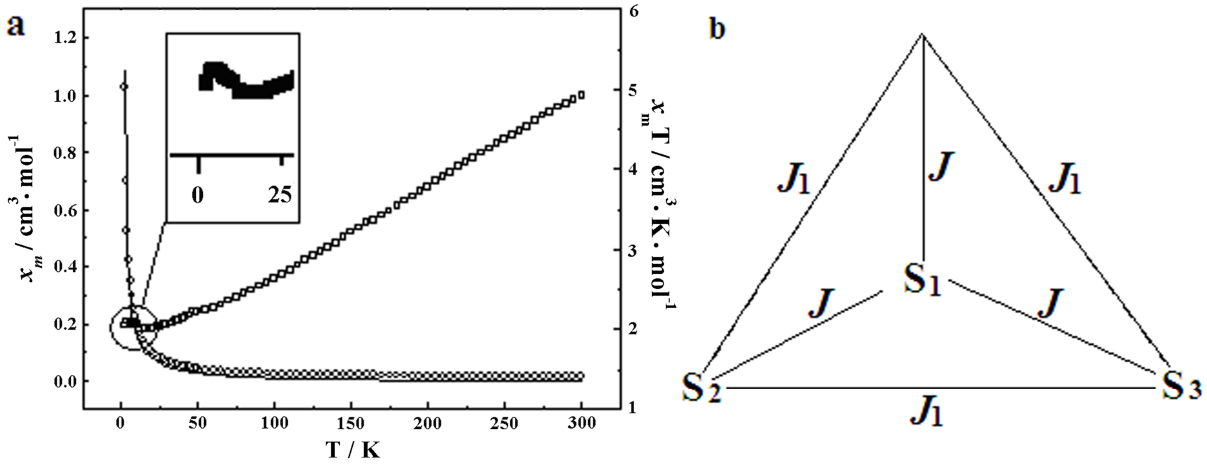

Figure 8. (a) The Plot of χ_M and $\chi_M T$ versus T for compound **1**. (b) The magnetic mode of tetra-nuclear copper (II) coordination fragment in compound 1.Schematic illustration of the synthesis routes of complexes.

Conclusion

In this paper, mixed ligand modified tetranuclear copper (II) complex, was firstly introduced into the Lindqvist-type clusters

as linking units to weave a fascinating 3D network structure, which exhibits a $4^{12}•6^3$-nbo (sodium chloride-type) topology. Cyclic voltammetric behavior of **1** exhibits three reduction waves and their oxidation counterpart in 1M H_2SO_4 aqueous solution, which can be ascribed to one-electron redox processes of Mo atoms and the redox processes of Cu(II) center. Furthermore, diffuse reflectivity spectrum of **1** shows its band gap being assessed as 3.02 eV, which could be applied as a wide gap semiconductor. Magnetic susceptibility study reveal predominant antiferromagnetic interactions between the Cu^{II} bridge units. The ongoing efforts will be concentrated on the organic–inorganic hybrid materials contained multinuclear coordination complex.

Acknowledgements

This work was supported the National Natural Science Foundation of China (Grants Nos. 21271056 and 21371042), the Ministry of Education and Specialised Research Fund for the Doctoral Program of Higher Education (20122329110001), the Natural Science Foundation of Heilongjiang Province(B201216), Key Laboratory of Functional Inorganic Material Chemistry (Heilongjiang University), Ministry of Education, Doctoral initiation Foundation of Harbin Normal University (No.KGB201214). Ministry of Education, Doctoral initiation Foundation of Harbin Normal University (No.KGB201214). Program for Scientific and Technological Innovation Team Construction in Universities of Heilongjiang Province (No. 2011TD010).

Notes and references

[a]*Key Laboratory for Photonic and Electronic Bandgap Materials, Ministry of Education, School of Chemistry and Chemical Engineering, Harbin Normal University, Harbin 150025, People's Republic of China; E-mail: hlyukai188@163.com(K.Yu); zhou_bai_bin@163.com(B.B.Zhou)*
[b]*Key Laboratory of synthesis of functional materials and green catalysis, Colleges of Heilongjiang Province, Harbin Normal University, Harbin, 150025, People's Republic of China;*
[c] *Faculty of Chemistry and Pharmacy, Jiamusi University, Jiamusi, HeilongJiang, 154007, People's Republic of China*

† Electronic Supplementary Information (ESI) available: Summary of selected bond lengths and angles; IR spectrum, PXRD patterns, UV-vis spectrum, XPS spectrum, TG curve, part structural figures of compounds **1**, and cif files of **1**. CCDC reference numbers: 708957 (**1**) See DOI: 10.1039/b000000x/

1 (a) P. Gouzerh, A. Proust, *Chem. Rev*., 1998, **98**, 77; (b) X. H. Yan, P. L. Zhu, J. B. Fei, J. B. Li, *Adv. Mater*. 2010, **22**, 1283.
2 (a) R. B. Getman, Y. S. Bae, C. E. Wilmer, R. Q. Snurr, *Chem. Rev*. 2012, **112**, 703; (b) M. P. Suh, H. J. Park, T. K. Prasad, D. W. Lim, *Chem. Rev*. 2012, **112**, 782; (c) J. R. Li, Y. Tao, Q. Yu, X. H. Bu, H. Sakamoto, S. Kitagawa, *Chem. Eur. J*. 2008, **14**, 2771.
3 (a) D. L. Long, E. Burkholder, L. Cronin, *Chem. Soc. Rev.*, 2007, **36**, 105; (b) C. Lydon, C. Busche, H. N. Miras, A. Delf, D. L. Long, L. Yellowlees, L. Cronin, *Angew. Chem. Int. Ed*., 2012, **51**, 2115; (c) Y. F. Zeng, X. Hu, F. C. Liu, X. H. Bu, *Chem. Soc. Rev.*, 2009, **38**, 469.
4 P. Horcajada, R. Gref, T. Baati, P. K. Allan, G. Maurin, P. Couvreur, G. Férey, R. E. Morris, C. Serre, *Chem. Rev*. 2012, **112**, 1232.
5 (a) P. Yin, C. P. pradeep, B. F. Zhang, F. Y. Lydon, C. Rosnes, M. H. Li, D. E. Bitterlich, L. Xu, L. Cronin, T. B. Liu, *Chem. Eur. J*. 2012, **18**, 8157; (b) M. Du, Y. M. Guo, S. T. Chen, X. H. Bu, S. R. Batten, J. Ribas, S. Kitagawa, *Inorg. Chem*., 2004, **43**, 1287.
6 (a) Y. G. Wei, B. B. Xu, C. L. Barnes and Z. H. Peng, *J. Am. Chem. Soc*., 2001, **123**, 4083; (b) B. B. Xu, Z. H. Peng, Y. G. Wei and D. R. Powell, *Chem. Commun*., 2003, 2562; (c) Y. Zhu, Z. C. Xiao, N. Ge, N. Wang, Y. G. Wei and Y. Wang, *Cryst. Growth Des*., 2006, **6**, 1620. (d) Q. Li, P. F. Wu, Y. G. Wei, Y. Xia, Y. Wang and H. Y. Guo, Z. Anorg. *Allg. Chem*., 2005, **631**, 773; (e) L. Xu, M. Lu, B. B. Xu, Y. G. Wei, Z. H. Peng and D. R. Powell, *Angew. Chem*., Int. Ed., 2002, **41**, 4129; (f) Q. Li, P. F. Wu, Y. G. Wei, Y. Wang, P. Wang and H. Y. Guo, *Inorg. Chem. Commun*., 2004, **7**, 524. (g) Y. G. Wei, B. B. Xu, C. L. Barnes and Z. H. Peng, *J. Am. Chem. Soc*., 2001, **123**, 4083.
7 M. X. Li, H. L. Chen, J. P. Geng, X. He, M. Shao, S. R. Zhu, and Z. X. Wang, *CrystEngComm*, 2011, **13**, 1687.
8 (a) A. Hashikawa, Y. Sawada, Y. Yamamoto, M. Nishio, W. Kosaka, Y. Hayashia, and H. Miyasaka, *CrystEngComm*, 2013, **15**, 4852; (b) V. Vrdoljak, B. Prugovečki, D. Matković-Čalogović, and J. Pisk, *CrystEngComm*, 2011, **13**, 4382.
9 G. S. Yang, H. Y. Zang, Y. Q. Lan, X. L. Wang, C. J. Jiang, Z. M. Su, and L. D. Zhu, *CrystEngComm*, 2011, **13**, 1461;
10 Z. Zhang, J. Yang, Y. Y Liu, and J. F. Ma, *CrystEngComm*, 2013, **15**, 3843.
11 (a) G. M. Sheldrick, SHELXL 97, Program for Crystal Structure Refinement, University of Göttingen, Germany, 1997; (b) G. M. Sheldrick, SHELXL 97, Program for Crystal Structure Solution, University of Göttingen, Germany, 1997.
12 I. D. Brown, D. Altermatt, *Acta Crystallographica. Section B, Structural Science*, 1985, **41**, 244.
13 Y. Wang, D.-R. Xiao, E.-B. Wang, L.-L. Fan, J. Liu, *Transition Met. Chem*., 2007, **32**, 950.
14 (a) E. Coronado, M. C. Giménez, C. J. Gómez-García, F. M. Romero, *Polyhedron*, 2003, **22**, 3115; (b) H. J. Jin, B. B. Zhou, C. M. Wang, Z. H. Su, Z. F. Zhao, Y. N. Zhang, C. C. Zhu, *Inorg. Chem. Commun*., 2009, **12**, 76.
15 C.D. Wagner, W.M. Riggs, L.E. Davis, J.F. Moulder and G.E. Muilenberg, Handbook of X-ray Photoelectron Spectroscopy, Perkin-Elmer Corp., MI, 1978.
16 Y. Xia, Y. G. Wei, Y. Wang, and H. Y Guo, *Inorganic Chemistry*, 2005, **44**, 9823.
17 (a) Z. M. Zhang, Y. F. Qi, C. Qin and E. B. Wang, *Inorg. Chem*., 2007, **46**, 8162; (b) Z. X. Li, H. Ma, S. L. Chen, Z. D. Pan, Y. F. Zeng, X. L. Wang, X. H. Bu, *Dalton Trans.*, 2011, **40**, 31.

Graphical Abstract

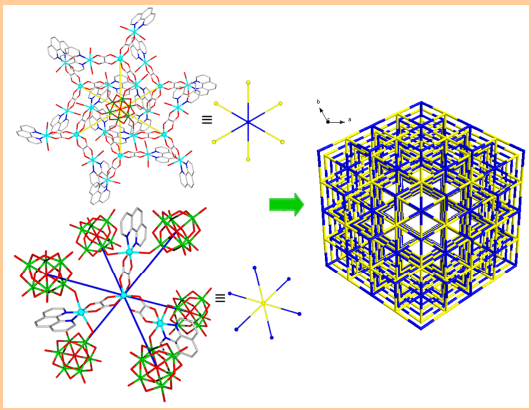

Mixed ligand modified tetranuclear copper (II) complex was firstly introduced into $\{Mo_6O_{19}\}$ systems as linking units to weave a fascinating 3D Bird's Nest-liked structure, which exhibits a $4^{12}\bullet6^3$-nbo (sodium chloride-type) topology. The compound display good redox properties, excellent semiconductive nature, and unique Magnetic activity.